Local Stochastic Vortex Structure Method for Synthetic Turbulence Computation in Flight Simulators

Jeffrey S. Marshall
The University of Vermont, Burlington, VT 05405

Rapid turbulence approximation on and around a vehicle is necessary for development of improved flight simulators for helicopters and aircraft, used both for pilot training and for video gaming applications. Predictions of synthetic turbulence methods must have both temporally and spatially accurate statistics compared to actual turbulence for the given turbulence mean velocity and Reynolds stress tensor. The stochastic vortex structure (SVS) method was recently proposed for turbulent flows with interacting particles, and shown to generate accurate statistical measures for homogeneous turbulence and for turbulent shear flows. Since the velocity in flight simulators is required only on target points near the flight vehicle, the current paper modifies the SVS method by (1) moving and rotating the vortex structures via stochastic differential equations and (2) introducing vortices only in a restricted vortex region surrounding the aircraft. This *local stochastic vortex structure* (LSVS) method decreases the SVS computational speed by several orders of magnitude, making it feasible for real-time turbulence computation in flight simulators. The proposed method is validated by comparing results for different statistical measures with predictions from direct numerical simulation (DNS) of homogeneous turbulence. Sensitivity of the different measures with numerical parameters in the LSVS model is examined.

Nomenclature

$\mathbf{A}$	=	vortex rotation matrix
$\mathbf{b}$	=	position vector of vortex blob centroid
$\mathbf{B}$	=	vortex blob amplitude vector
C	=	forcing coefficient
D	=	Lagrangian structure function
D_{ij}	=	rate of deformation tensor (symmetric part of velocity gradient)
D_V	=	width of the vortex domain
f	=	frequency
$\bar{\mathbf{f}}_F$	=	small-wavenumber forcing vector
$\mathbf{F}$	=	force vector in Fourier-transformed Navier-Stokes equations
k	=	wavenumber magnitude
$\mathbf{k}$	=	wavenumber vector
ℓ_0	=	turbulence integral length scale
L	=	vortex length
M	=	number of target points
M_T	=	number of uniformly-spaced test points on a sphere
N_b	=	number of vortex blobs per vortex structure
n_V	=	number of vortices per unit volume
N_V	=	number of vortices
P	=	incomplete gamma function
$\mathbf{P}$	=	projection operator for Fourier transformed Navier-Stokes equations
q	=	turbulence kinetic energy
r	=	displacement used for Eulerian structure function
R_{ij}	=	Reynolds stress tensor
$\mathbf{s}$	=	displacement vector used in Biot-Savart equation
s	=	magnitude of $\mathbf{s}$
s_n	=	dimensionless Eulerian longitudinal structure function of order n
S_n	=	Eulerian longitudinal structure function of order n
Δt	=	time step
t	=	time
t_{0n}	=	time at which nth vortex structure is initiated
t_n	=	dimensionless Eulerian longitudinal structure function of order n
T_n	=	Eulerian transverse structure function of order n
T_L	=	turbulence integral time scale
T_0	=	eddy turn-over time scale
T_V	=	vortex life time
u_0	=	turbulence root-mean-square velocity
u_i	=	fluctuation velocity components
$\mathbf{U}$	=	mean velocity vector

U_x = translation speed of target points

W_{ij} = vorticity tensor (skew-symmetric part of velocity gradient)

v = vortex translation velocity

x = centroid position vector for vortex structure

y = position vector of target point

$\alpha_1, \alpha_2, \alpha_3$ = proportionality coefficients (Eq. (2))

β = vortex blob overlap coefficient

Γ_n = strength of *n*th vortex

δ = vortex core radius

ε = rate of turbulence dissipation per unit volume

$\varepsilon_1, \varepsilon_2, \varepsilon_3, \eta_E$ = Euler parameters

$\boldsymbol{\zeta}_n$ = orientation vector of *n*th vortex

η = turbulence Kolmogorov length scale

ν = fluid kinematic viscosity

$d\xi$ = Gaussian distributed random variable with variance Δt

ρ = autocorrelation function

σ_v = variance of fluctuating velocity

τ = lag time in autocorrelation function

τ_n = age of *n*th vortex structure

τ_{0n} = age of *n*th vortex at formation

ω = vorticity vector

Ω = rotation rate of vortex structure

I. Introduction

Problems involving synthetic turbulence generation on an object in a turbulent flow are important for operation of flight simulators, used for military and commercial pilot training and for video gaming applications. Flight in turbulent flow conditions is particularly important in activities such as landing a helicopter on a ship [1,2], for which the turbulence structure is anisotropic, inhomogeneous and sensitive to the wind direction relative to the ship. In such applications, the synthetic turbulence generation must be sufficiently rapid to run in real-time and it must be both temporally and spatially consistent with actual turbulence.

The turbulent fluctuations on a Lagrangian particle in a turbulent flow can be well modeled using a stochastic Lagrangian method (SLM) [3,4], in which a stochastic differential equation is solved for each component of the fluctuating velocity field. The SLM approach is a rapid and accurate method which is widely used for simulation of turbulence in particulate flows [5]. However, while SLM can accurately simulate turbulence time scales, it's inability to accurately generate structural features of turbulence makes SLM unsuitable to this application [6]. There are two reasons for this statement. First, in many flight simulator applications, it is desired to know the velocity at more than one point around the object. For instance, to compute the moments acting on an aircraft one would need to know the fluid velocity field on a small stencil of points surrounding the vessel. The correlation between the fluctuating velocities on this stencil cannot be accurately generated using an SLM approach because in SLM the stochastic forcing at nearby points is not correlated, unlike the case in real turbulence. Since the moments depend on the difference in these local velocities, they are very sensitive to errors associated with lack of correlation in the SLM approach. Secondly, the turbulence time scales observed by the

moving object depend in part on the velocity of the object through the fluid, which in turn requires knowledge of the spatial structure of the turbulence.

A variety of other synthetic turbulence methods have been developed for estimation of inlet and initial conditions for large-eddy simulation and discrete-eddy simulation calculations [7-9]. Synthetic turbulence approaches [10,11] represent the turbulence using a random velocity field that is constrained to be incompressible and that when averaged, yields mean Reynolds stress quantities that are consistent with desired values, e.g., such as those computed using a Reynolds-Averaged Navier-Stokes (RANS) simulation method. For convenience, the velocity fluctuations are typically assumed to have a normal distribution. Huang et al. [12] showed that previous synthetic turbulence methods yield an incorrect energy spectrum, and they proposed a new approach to generate a flow field with the correct spectrum. A review of synthetic turbulence methods is given by Tabor and Baba-Ahmadi [13], with particular focus on inlet flow conditions for large eddy simulation.

One shortcoming of existing synthetic turbulence models for simulation of turbulence on a moving body is that these models typically do not accurately predict the coherent eddy structures of the turbulent flow. The scaling and structure of coherent vortices was examined by Jiménez et al. [14] in homogeneous turbulence based on results of high-resolution direct numerical simulations (DNS) and by Berlin et al. [15] in a turbulent shear flow using experiments with low-temperature helium gas. Both studies found that the turbulent vorticity field is dominated by a set of strong (coherent) vortices of finite length and with tubular shape, surrounded by a sea of weak random (non-coherent) vorticity. The length and core radius of the coherent vortices were found to scale with the Lagrangian integral length scale and the Kolmogorov length scale, respectively, and the vortex strength was found to scale with the

square root of the microscale Reynolds number. An early theoretical model of turbulence as a collection of Burgers vortices was proposed by Townsend [16], and further analyses of the statistical properties of this and related vortex systems are given by Refs. [17-21]. Kivotides and Leonard [22] report results of a computation in which homogeneous turbulence is represented by a set of finite-length vortex structures, and show that this system generates an energy spectrum that satisfies the Kolmogorov $k^{-5/3}$ scaling in the turbulence inertial range. Extensions of the vortex filament method were presented by Peter Bernard's group for turbulent mixing layers [23], co-flowing jets [24], and turbulent boundary layers [25], which demonstrated highly successful comparisons between the vortex filament representations and data from experimental and direct numerical simulations.

Recent work utilizing a vortex structural representation for turbulent transport of a particulate fluid with large number of interacting particles was proposed by Ayyalasomayajula et al. [26], who proposed a model in which turbulent eddies are represented by a two-dimensional vortex array and a stochastic algorithm is used to vary the strength of each vortex in time. This simple model was shown to yields reasonable results for particle acceleration statistics and clustering. A three-dimensional *stochastic vortex structure* (SVS) model was proposed by Sala and Marshall [6] for prediction of turbulent particle transport. In this model, the turbulent vorticity field is approximated by a set of finite-length, fixed vortex structures which are randomly positioned and oriented in the flow field. Unlike the vortex filament method, the SVS method does not use the vortex structures to evolve the flow field; rather, they are used as a kinematic representation to approximate a subgrid-scale synthetic turbulence to use for particle evolution in a flow with a given Reynolds stress distribution. An accelerated version of the SVS model was recently developed by Dizaji and Marshall [27] using the fast multipole method.

Predictions of the SVS model for particle collision rate were found to be in close agreement with DNS predictions of homogeneous turbulence for a wide range of fluid and particulate measures, including turbulence energy spectrum, probability density functions for velocity, acceleration and vorticity, particle collision rate, and fractal dimension and size distributions of agglomerates formed of adhesive particles. The SVS method was applied to particle transport in anisotropic, inhomogeneous turbulence by Dizaji et al. [28], which proposed an inverse procedure by which the vortex orientations can be specified to yield a given Reynolds stress field.

The SVS formulations for particulate flows compute the synthetic fluctuating velocity field on all points of a grid covering the computational domain, and then interpolate the fluid velocity onto a set of particles transported by the flow. The vortex structures are transported and rotated by the induced flow field, obtained by interpolation from the computational grid. While this formulation of the SVS method is suitable for simulations of particulate fluids with a large number of particles spread out over the flow domain, it requires computation of the fluctuating velocity on a large number of grid points and is therefore inefficient for simulating turbulence on a small number of target points near a single object traversing the flow field. In the current paper, we present a new *localized stochastic vortex structure* (LSVS) method that is designed for rapidly generating synthetic turbulence in the vicinity of a single object traveling through a turbulent flow. The LSVS method is described in Section 2 of the paper. In Section 3, we validate this method against DNS results for an object in a homogeneous turbulent flow. Conclusions are given in Section 4.

II. Synthetic Turbulence Simulation with Stochastic Vortex Structures

We seek to develop a rapid, statistically-accurate method for constructing a synthetic fluctuating fluid velocity field characteristic of that acting on an object traversing a turbulent flow. It is assumed that the Reynolds stress distribution in the turbulent flow is known (e.g., via a prior RANS simulation), and for convenience it is assumed that the turbulence is statistically stationary. In addition to the simulation being rapid, we desire that the synthetic turbulence field possess the following properties:

- that the velocity field be incompressible;
- that the fluctuating velocity is consistent with the $k^{-5/3}$ Kolmogorov scaling of the power spectrum in the inertial range for homogeneous turbulence;
- that it is consistent with the observed Gaussian distribution for the probability density function (p.d.f.) of the velocity field and with the fat-tail distribution [29] of the p.d.f. of the acceleration field;
- that it correctly predicts the two-point velocity correlation in the turbulent flow; and
- that Reynolds stress distribution induced by the synthetic fluctuating velocity field is consistent with the prescribed Reynolds stress distribution used to initialize the vortex structures.

The first of these properties is identically satisfied from the use of the Biot-Savart equation to compute the induced velocity. The second and third of these properties has been demonstrated for the stochastic vortex structure (SVS) method in homogeneous isotropic turbulence by Refs. [6, 27], exhibiting excellent agreement between the SVS method predictions and results of direct numerical simulations (DNS). The fourth property has not yet been directly established, but hints that the SVS method might be consistent with this property are apparent from the results of Ref.

[27], who showed that the SVS method correctly predicts the vorticity p.d.f. distribution in homogeneous turbulence and that the method also correctly predicts particle collision rate and formation of particle agglomerates, all of which depend on accurate prediction of relative velocity at two nearby points. We will examine this fourth property further in the present paper. The fifth property was examined by Ref. [28], who developed and validated an inverse technique that can be used to set vortex orientation and strengths to correctly reproduce a given (anisotropic) Reynolds stress field for turbulent shear flows.

The previous papers written using the SVS method have focused on flows with large number of particles spread throughout the flow field. The SVS method computed the synthetic turbulent flow on all points of a Cartesian grid covering the flow, and then this fluctuating fluid velocity was interpolated onto the Lagrangian particles. A fast multipole method (FMM) developed for acceleration of the velocity calculation in the SVS method proposed for particulate flows was designed explicitly for estimating the synthetic velocity throughout the flow field, and was found to provide over two orders of magnitude reduction in computational time for the velocity field with negligible error [27]. This FMM acceleration method would not be efficient if applied to the problem addressed in the current paper, however, in which we desire to estimate the synthetic velocity on a small set of points which are closely clustered in space. Similarly, the method by which the vortex structures are transported using the computed velocity field on the grid covering the flow field would not be efficient for the current problem, as it would necessitate computing the fluctuating velocity not only on a small set of clustered points, but everywhere over the computational grid. The primary focus of the current paper is to develop a new localized stochastic vortex structure (LSVS) model can be used to rapidly generate synthetic

velocity fluctuations satisfying the above set of properties on a small set of closely clustered target points.

A. Localized Stochastic Vortex Structure Method

The stochastic vortex structure model generates the synthetic fluctuating velocity field **u** induced by a collection of vortex structures placed and oriented randomly within the flow field. Since in the current paper we are interested only in the fluctuating velocity on a small set of clustered target points, located at positions $\mathbf{y}_m(t)$, $m = 1,...,M$, we are primarily interested in vortex structures that are in some sense close to the target points. To accelerate the computation, in the LSVS method the vortex structures are introduced only in a *vortex domain* which surrounds the target points (Figure 1). The vortex domain moves within the computational domain, such that vortices that move out of one side of the vortex domain are bounced to the opposite side of the vortex domain.

The distribution of the vortex orientation vector $\boldsymbol{\zeta}_n$ and the vortex strength Γ_n are adjusted according to the specified Reynolds stress field, where $n = 1,\ldots, N_V$ for a system with N_V vortex structures. In the simplest version of the SVS method, the vortex structures all have the same finite length L and core radius δ. The vortex length L is typically assumed to be of the order of the turbulence integral length scale $\ell_0 \sim u_0^{\,3}/\varepsilon$, where u_0 is the turbulence root-mean-square velocity and ε is the turbulence dissipation rate [30]. Kambe and Hatakeyama [31] used a scaling analysis to show that the vortex core radius δ is proportional to the Kolmogorov length scale $\eta = (\nu^3/\varepsilon)^{1/4}$, where ν is the kinematic viscosity. This result is in agreement with experimental and numerical results [14,15], which yield an estimate $\delta \cong 3.9\eta$ for the large-scale

coherent vortex structures. Each vortex structure has a lifetime T_V, which is assumed to be proportional to the integral time scale T_L. A rough estimate for the integral time is given by the eddy-turnover time scale $T_0 = \ell_0 / u_0$. Using the scaling estimate $\ell_0 \sim u_0^3 / \varepsilon$ and setting the turbulent kinetic energy for homogeneous turbulence as $q = (3/2)u_0^2$, we can write

$$T_0 = \frac{2q}{3\varepsilon}. \tag{1}$$

In the SVS method, the length L, core radius δ and life span T_V of the vortex structures can therefore be expressed as

$$L = \alpha_1 \ell_0, \qquad \delta = \alpha_2 \eta, \qquad T_V = \alpha_3 T_0, \tag{2}$$

where α_1, α_2 and α_3 are proportionality coefficients whose values will be determined by comparison of the LSVS predictions with DNS data.

The age of a vortex structure, $\tau_n(t)$, is determined starting from an initial age τ_{0n} by

$$\tau_n = \tau_{0n} + t - t_{0n}. \tag{3}$$

Here, t is the current time and t_{0n} denotes the time at which the vortex structure was initiated. Vortex structures initiated at the start of the computation are assigned a random initial age by setting τ_{0n} / T_V equal to a random variable with uniform probability distribution between 0 and 1.

For vortex structures introduced later in the calculation, τ_{0n} is set equal to zero. When the vortex age $\tau_n(t)$ exceeds the specified vortex lifespan T_V, the vortex structure is removed and a new vortex structure is introduced with random position within the vortex domain. The vortex initial strength and orientation is determined by the prescribed Reynolds stress at the new vortex location using the inverse method described in Ref. [28].

B. Motion of Vortex Structures

In the SVS method for particulate fluids developed in our previous work [27, 28], each vortex structure is translated and rotated by the sum of the mean velocity and the induced fluctuating velocity at the vortex endpoints, and then the vortex structure is normalized to the prescribed length L at the end of each time step. Since this method for moving the vortex structures requires knowledge of the velocity at a large number of points within the vortex domain, it is too time-consuming for the objectives of the current localized stochastic vortex structure method.

As an alternative, in the localized stochastic vortex structure method we solve for the fluctuating translation velocity **v** of each vortex structure by solution of a stochastic differential equation of the Langevin form

$$dv_i = -\frac{v_i}{T_0}dt + \left(\frac{4q_i}{T_0}\right)^{1/2} d\xi \qquad \text{(no sum on } i\text{)}, \tag{4}$$

where q_i is the turbulence kinetic energy associated with the i^{th} velocity component and the differential $d\xi$ is a Gaussian distributed random variable with zero mean and variance equal to

the time step Δt. The initial condition for the vortex fluctuating velocity is $v_i(\mathbf{x},0) = \sigma_v d\xi$, where $\sigma_v = \sqrt{2q_i/3}$ is the velocity variance. Eq. (4) is of the same form as the Thomson [4] stochastic Lagrangian model for turbulence fluctuations, and it is commonly used to model turbulent fluctuations in particle dispersion processes. The centroid position vector **x** for each vortex structure is obtained by solving

$$\frac{dx_i}{dt} = v_i + U_i, \tag{5}$$

where U_i are the components of the prescribed mean velocity vector evaluated at the vortex centroid.

The rotation rate $\mathbf{\Omega}$ of the vortex structures is similarly modeled using a stochastic differential equation of the form

$$d\Omega_i = -\frac{\Omega_i}{T_0} dt + \left(\frac{4q_i}{T_0 \ell_0^2} \right)^{1/2} d\xi \quad \text{(no sum on } i\text{)}, \tag{6}$$

where ℓ_0 and T_0 are the turbulence integral length and the eddy turnover time scale defined previously. The net rotation rate $\hat{\mathbf{\Omega}}$ of the vortex orientation vector is defined by

$$\hat{\Omega}_i = \Omega_i + D_{ij}\zeta_j + W_{ij}\zeta_j - D_{jk}\zeta_j\zeta_k\zeta_i, \tag{7}$$

where D_{ij} and W_{ij} are the components of the rate of deformation tensor and the vorticity tensor of the mean velocity field, defined by

$$D_{ij} = \frac{1}{2}\left(\frac{\partial U_i}{\partial x_j} + \frac{\partial U_j}{\partial x_i}\right), \qquad W_{ij} = \frac{1}{2}\left(\frac{\partial U_i}{\partial x_j} - \frac{\partial U_j}{\partial x_i}\right). \tag{8}$$

The vortex orientation vector is rotated from its initial value $\boldsymbol{\zeta}_0$ by the rotation

$$\boldsymbol{\zeta} = \mathbf{A} \cdot \boldsymbol{\zeta}_0 . \tag{9}$$

The rotation matrix **A** can be written in terms of the Euler parameters ε_1, ε_2, ε_3 and η_E as

$$\mathbf{A} = \begin{bmatrix} 1-2\left(\varepsilon_2^2+\varepsilon_3^2\right) & 2\left(\varepsilon_1\varepsilon_2+\varepsilon_3\eta_E\right) & 2\left(\varepsilon_1\varepsilon_3-\varepsilon_2\eta_E\right) \\ 2\left(\varepsilon_2\varepsilon_1-\varepsilon_3\eta_E\right) & 1-2\left(\varepsilon_3^2+\varepsilon_1^2\right) & 2\left(\varepsilon_2\varepsilon_3+\varepsilon_1\eta_E\right) \\ 2\left(\varepsilon_3\varepsilon_1+\varepsilon_2\eta_E\right) & 2\left(\varepsilon_3\varepsilon_2-\varepsilon_1\eta_E\right) & 1-2\left(\varepsilon_1^2+\varepsilon_2^2\right) \end{bmatrix}, \tag{10}$$

where by definition

$$\varepsilon_1^2 + \varepsilon_2^2 + \varepsilon_3^2 + \eta_E^2 = 1 . \tag{11}$$

The rate of change of the Euler parameters can be expressed in terms of the components of the total rotation rate $\hat{\boldsymbol{\Omega}}$ as [32]

$$\begin{bmatrix} d\varepsilon_1/dt \\ d\varepsilon_2/dt \\ d\varepsilon_3/dt \\ d\eta_E/dt \end{bmatrix} = \frac{1}{2}\begin{bmatrix} \eta_E\hat{\Omega}_x - \varepsilon_3\hat{\Omega}_y + \varepsilon_2\hat{\Omega}_z \\ \varepsilon_3\hat{\Omega}_x + \eta_E\hat{\Omega}_y - \varepsilon_1\hat{\Omega}_z \\ -\varepsilon_2\hat{\Omega}_x + \varepsilon_1\hat{\Omega}_y + \eta_E\hat{\Omega}_z \\ -\varepsilon_1\hat{\Omega}_x - \varepsilon_2\hat{\Omega}_y - \varepsilon_3\hat{\Omega}_z \end{bmatrix}. \quad (12)$$

C. Initial Vortex Structure Orientation

Vortex structures are initially placed within the vortex domain at the start of the computation, and new vortex structures are also initiated within the vortex domain when an existing vortices structure is removed because its age has increased past the allowed vortex lifespan. When a new vortex structure is initialized, it is necessary to specify both its strength and orientation. The vortex strength must be set to be consistent with the local turbulence kinetic energy, and the vortex orientation must be initialized to be consistent with the structure of the local prescribed Reynolds stress tensor $R_{ij} = \overline{u_i u_j}$, where **u** is the fluctuating velocity field induced by the vortices and an overbar denotes a time average. Dizaji and Marshall [27] note that the turbulent kinetic energy can be expressed as a linear function of the product $n_V \Gamma^2$, where n_V is the number of vortices per unit volume and Γ is the vortex strength, which is also in agreement with the theoretical finding of Saffman [20]. Thus, by selecting a value for n_V and given a prescribed turbulent kinetic energy field, the value of vortex strength can be obtained. The effect of number of vortices on the accuracy of the SVS predictions was examined in Refs [27, 28], who find that the results generally improve as n_V increases, but that a value of n_V

greater than about 4 (corresponding to about 1000 vortices in a computational domain with volume $(2\pi)^3$) is generally sufficient to yield accurate results in comparison to DNS.

The orientation distribution of the vortex structures is used to adjust the degree of anisotropy of Reynolds stress tensor. We begin by computing a set of $M_T = 642$ evenly-spaced *test points* on the surface of a unit sphere by dividing the faces of an icosahedron a prescribed number of times and projecting the vertices to the unit sphere. These test points are used to generate a set of randomly-oriented unit vectors with uniform probability distribution in three-dimensional space. For isotropic turbulence, as considered in the current paper, the vortex orientation vector is obtained by randomly selecting one of the test points on the unit sphere, and then setting the vortex orientation equal to the radial vector to the selected test point. For anisotropic turbulence, the vortex structure orientation is set using the inverse procedure described by Dizaji et al. [28].

D. Velocity Calculation

The velocity computation is done by first pre-computing the velocity induced by a vortex structure of unit strength on the *data plane*, which is defined as the positive *r-z* plane relative to the axis of the vortex structure (Figure 2). This computation is performed once at the beginning of the computation and the results are stored. The induced velocity on the data plane is determined by computing the induced velocity normal to the *r-z* plane of a coordinate system that is local to a vortex structure of unit strength, where the vortex center is located at the origin of the local coordinate system. The velocity at each point of the grid used to cover the data plane is determined by integration of the Biot-Savart integral using a Gaussian vortex blob method [33], where the number of vortex blobs N_b used to discretize the vortex structure is set equal to

$N_b = \text{int}(\beta L/\delta)$. The Gaussian radius of the blob is set equal to the vortex structure radius δ and β is a blob overlap coefficient. If the centroid of the i^{th} vortex blob is denoted by $\mathbf{b}_i$, $i = 1,..., N_b$, the associated vorticity field is given by

$$\boldsymbol{\omega}_i(\mathbf{x},t) = \frac{\mathbf{B}_i}{\pi^{3/2}\delta^3}\exp\left(-\frac{|\mathbf{x}-\mathbf{b}_i|^2}{\delta^2}\right), \tag{13}$$

where the blob amplitude $\mathbf{B}_i$ is given by $\mathbf{B}_i = (L/N_b)\,\mathbf{e}_z$. Substituting (13) into the Biot-Savart integral

$$\mathbf{u}(\mathbf{x},t) = -\frac{1}{4\pi}\int_V \frac{\mathbf{s}\times\boldsymbol{\omega}(\mathbf{x}',t)}{s^3}\,dv', \tag{14}$$

where $s \equiv |\mathbf{s}| \equiv |\mathbf{x}-\mathbf{x}'|$, and performing the integration yields the velocity $\mathbf{u}_i$ induced by the i^{th} vortex blob at a point $\mathbf{x} = r\mathbf{e}_r + z\mathbf{e}_z$ on the data plane as

$$\mathbf{u}_i(\mathbf{x},t) = \frac{P\left(\frac{3}{2},\frac{|\mathbf{x}-\mathbf{b}_i|^2}{\delta^2}\right)}{4\pi|\mathbf{x}-\mathbf{b}_i|^3}\;\boldsymbol{\Omega}_i\times(\mathbf{x}-\mathbf{b}_i), \tag{15}$$

where $P(a,z)$ is the incomplete gamma function with limits $P(a,0)=0$ and $P(a,\infty)=1$. When $a = 3/2$ and $z = x^2$ for some real variable x, a convenient expression for the incomplete gamma function in terms of the error function erf(x) can be written as [34]

$$P(\tfrac{3}{2}, x^2) = \mathrm{erf}(x) - \frac{2xe^{-x^2}}{\sqrt{\pi}}. \tag{16}$$

The velocity at any point on the data plane is obtained by summing the velocity induced by all N_b vortex blobs.

Once the induced velocity of the unit vortex is obtained on the data plane, the induced velocity from a vortex structure m at target point $\mathbf{y}$ is obtained at subsequent times by interpolation from the data plane. This interpolation is performed by centering the data plane at the vortex structure centroid $\mathbf{x}_m$ and orienting the plane so that it passes through the target point $\mathbf{y}$ and is tangent to the vortex axis unit vector $\boldsymbol{\zeta}_m$, as illustrated in Figure 2. Repeating this procedure for all vortices in the vortex domain and adding the induced velocity from each yields the induced velocity on a selected target point.

III. Validation for Homogeneous Turbulence

In this section we examine the induced velocity on a set of target points in a homogeneous turbulent flow, comparing measures of the flow fluctuations at the target points computed using the LSVS method with predictions obtained from direct numerical simulation (DNS) of the turbulent flow.

The DNS computations of isotropic, homogeneous turbulence used for validation were performed using a pseudo-spectral method on a 128^3 triply-periodic grid with second-order Adams-Bashforth time stepping and exact integration of the viscous term [35]. In this approach,

the spectral Navier-Stokes equations are evolved in time after having been projected onto a divergence-free space using the operator $P_{ij} = k_i k_j / k^2 - \delta_{ij}$ according to the expression

$$\overline{\mathbf{u}}^{n+1} = \overline{\mathbf{u}}^{n} \exp(-\nu k^2 \Delta t) + \Delta t \, \mathbf{P} \cdot \left[\frac{3}{2} \overline{\mathbf{F}}^{n} \exp(-\nu k^2 \Delta t) - \frac{1}{2} \overline{\mathbf{F}}^{n-1} \exp(-2\nu k^2 \Delta t) \right], \tag{17}$$

where an overbar denotes Fourier transform in three space dimensions, a superscript indicates the time step, ν is the kinematic viscosity, and **k** is the wavenumber vector with magnitude *k*. The force vector **F** on the right-hand side has Fourier transform given by

$$\overline{\mathbf{F}} = \overline{\mathbf{u} \times \boldsymbol{\omega}} + \bar{\mathbf{f}}_F, \tag{18}$$

where $\bar{\mathbf{f}}_F$ is the small wavenumber forcing term required to maintain the turbulence with approximately constant kinetic energy. The velocity field was made divergence-free at each time step by taking its Fourier transform and using the spectral form of the continuity equation, given by

$$\mathbf{k} \cdot \overline{\mathbf{u}} = 0. \tag{19}$$

Anti-aliasing of the DNS computations was performed using the standard approach of truncating the coefficients of the highest 1/3rd wave numbers. The forcing vector was assumed to be proportional to the fluid velocity [36, 37], such that

$$\bar{\mathbf{f}}_F = \begin{cases} C\bar{\mathbf{u}} & \text{for } k < k_{crit} \\ 0 & \text{for } k > k_{crit} \end{cases}, \tag{20}$$

where the coefficient C was set equal to $C = 0.0045 / E_{low}$ and $E_{low} = \frac{1}{2} \sum_{k<k_{crit}} \bar{\mathbf{u}} \cdot \bar{\mathbf{u}}$ is the kinetic energy in all modes with wavenumber amplitude $k < k_{crit}$. The current computations were performed with $k_{crit} = 5$, so that the forcing acts only on the large-scale eddies. Various measures of the DNS turbulence are recorded in Table 1.

The results of the LSVS computations depend on the values of the proportionality coefficients α_1, α_2 and α_3 defined by (2), the number of vortices N_V, the vortex strength Γ, and the width D_V of the vortex domain. It was demonstrated in Ref. [27] that for a given computational domain, the value of turbulent kinetic energy is proportional to the product $N_V \Gamma^2$. In the current computations, we set $N_V \Gamma^2 = 250$ in order to match the turbulent kinetic energy in the DNS and LSVS computations. A 'standard' LSVS computation was selected with $N_V = 512$ vortices in a vortex region with half-width $D_V = 2.4$ centered on the middle target point. Vortices whose centers leave this region were bounced back to the other side of the vortex region. In cases with moving target points, the vortex region is translated with the target points. The proportionality coefficients for this standard computation were set as $\alpha_1 = 1$, $\alpha_2 = 8$, and $\alpha_3 = 3$ based on fitting with the DNS data. Sensitivity of the predictions to these parameters will be discussed.

The computations were performed with 101 target points aligned in a straight line parallel to the *x*-axis with separation distance $\Delta x = 0.01$ between each point. The time step for both the

LSVS and DNS methods was set equal to $\Delta t = 0.005$, and both runs were performed for 40,000 time steps. The LSVS computations (including post-processing) required a CPU time of approximately 0.014 s per time step, versus 3.6 s per time step for the DNS computations, indicating a speed-up by a factor of over 250 with LSVS versus DNS even on a single-CPU workstation. This speed-up would increase dramatically in a highly parallelized computation since the vortex-based computations can easily be parallelized by assigning vortices to different processors [38], whereas spectral DNS computations are much more difficult to parallelize. The speed-up with LSVS would also be much greater for problems with anisotropic turbulence in which the highly efficient triply-periodic spectral DNS code cannot be used.

A plot of the CPU time for the LSVS computations (not including post-processing) per time step per target point is shown as a function of number of vortices in Figure 3. The figure shows clearly that the CPU time varies linearly with number of vortices. As an example for computations with $N_V = 512$ vortices, as used in the validation study in the current paper, the LSVS computation requires 38 μs per target point per time step. One of the nice features of the LSVS method is that there are no stability limitations on the time step. Assuming a frame rate of 60 Hz (and a corresponding time step of 1/60 s) for the flight simulator, our computations indicate that the turbulence field could be computed in real time for up to about 440 target points. This example indicates that real-time operation for flight simulators is quite feasible with the proposed LSVS synthetic turbulence method, even with running on a standard single-processor computer.

A. Stationary Target Points

Computations with stationary target points locations were examined extensively to determine accuracy of the SVS approach and sensitivity to the various numerical parameters. Time series showing the *x*-component of the fluctuating velocity field at the first target point for both the DNS and LSVS computations are shown in Figure 4. The ratio of kurtosis divided by the variance squared is equal to 2.70 and 3.37 for the DNS and LSVS computations, respectively, which compares reasonably well with the value 3 for a normally distributed stochastic process. The probability density function of the *x*-component of the fluctuating velocity, non-dimensionalized by its root-mean-square value, is plotted in Figure 5. The open square symbols are obtained from the LSVS computation and the filled deltas are from the DNS computation. As is typical of turbulent velocity fields, both sets of velocity data are reasonably well fit by a Gaussian function, given in the figure by a solid line. The power spectrum $e(f)$ for both LSVS and DNS predictions is plotted in Figure 6 as a function of fluctuation frequency *f*. In the inertial range, both sets of data exhibit a good fit to the expected variation $e \propto f^{-5/3}$, which results from the Kolmogorov power spectrum together with the Taylor frozen turbulence assumption [18]. The DNS and LSVS predictions deviate at high frequency ($f > 30$), which is expected as the LSVS assumption of vortex structure of a single size was targeted to capture turbulence scaling only within the inertial range. The p.d.f. and spectral plots described above were examined for LSVS computations with a wide range of different values of the numerical parameters, including the coefficients α_1, α_2 and α_3 and the number of vortices N_V. The computed results exhibited little sensitivity to the value of these parameters.

The autocorrelation function $\rho(\tau)$ of the *x*-component of velocity is defined by

$$\rho(\tau) \equiv \langle u(t)\,u(t+\tau)\rangle / \langle u^2(t)\rangle, \tag{21}$$

where $u(t)$ denotes the fluctuating fluid velocity at the first target point in the x-direction at time t and brackets denote a time average over the computational time. The autocorrelation function is plotted for the LSVS and DNS data in Figure 7a as a function of the lag time τ. The integral time scale is defined with respect to the velocity autocorrelation as

$$T_L \equiv \int_0^\infty \rho(\tau)\, d\tau \,. \tag{22}$$

The computed integral times scales are obtained from (22) as 2.7 for the DNS predictions and as 2.2 for the LSVS predictions. The dashed line in Figure 7a indicates the common expression of autocorrelation for a stationary Gaussian process [39]

$$\rho(\tau) = \exp(-\tau / T_L)\,, \tag{23}$$

which is computed using the DNS integral time scale T_L. The approximation (23) is seen to be a reasonable fit to both the DNS and LSVS computational data. The second-order Lagrangian structure function $D(\tau)$, defined by

$$D(\tau) \equiv \left\langle [u(t+\tau) - u(t)]^2 \right\rangle / \left\langle u^2(t) \right\rangle, \tag{24}$$

is plotted in Figure 7b for both the LSVS and DNS computations. The dashed curve in this plot represents the theoretical estimate

$$D(\tau) = 2[1 - \rho(\tau)] = 2[1 - \exp(-\tau / T_L)], \tag{25}$$

where the expression (23) is used in the second equation of (25).

Time variation of the fluid velocity on stationary target points in the LSVS computations can occur from three different effects – (1) death of vortices and birth of new vortices, (2) translation and rotation of the vortices, and (3) bouncing of vortices that leave one side of the vortex region onto the opposite side of the vortex region. Sensitivity of the predicted autocorrelation function for LSVS computations at stationary target points is examined in Figure 8. In Figure 8a, the predicted autocorrelation function is compared for three different values of the vortex lifetime, corresponding to $\alpha_3 = 1$, 3 and 5. We see that the autocorrelation function is highly sensitive to the value of the prescribed vortex lifetime, with the best match to DNS data for $\alpha_3 = 3$ (as shown in Figure 7). In Figure 8b, sensitivity of the autocorrelation function to vortex motion is evaluated by comparing predictions with full vortex motion to results of a computation with no vortex motion and to the results of a computation with vortex translation, but no rotation. The autocorrelation function is found to be substantially more sensitive to vortex translation than it is to vortex rotation. Finally, in Figure 8c we examine sensitivity of the autocorrelation function to vortex bouncing between the sides of the vortex region by comparing predictions with and without vortex bouncing. The predictions for the two cases are found to be very close, indicating a low level of sensitivity to vortex bouncing for stationary target points, at least for the size of the vortex region used in these computations.

The Eulerian longitudinal structure function of order n, $S_n(r)$, is defined by

$$S_n(r) = \left\langle \Delta u(r)^n \right\rangle, \tag{26}$$

where $\Delta u(r) = u(x+r,t) - u(x,t)$. The Eulerian longitudinal structure function was computed as a function of offset distance *r* for orders *n* = 2, 4, 6, 8, and 10. We found that $S_n(r)$ is almost unaffected by change in the vortex lifetime T_V, but that it is sensitive to the value of the vortex core radius δ. For instance, the predicted value of $S_n(r)$ from DNS is compared to LSVS predictions in Figure 9 for cases with $\alpha_2 = 4$ and $\alpha_2 = 8$ on log-log plots. The LSVS results with $\alpha_2 = 4$ are observed to be significantly higher than the DNS predictions, particularly for larger values of *n*. The LSVS predictions with $\alpha_2 = 8$ are in excellent agreement to the DNS predictions for all values of *n* examined.

The Eulerian transverse structure function of order *n*, $T_n(r)$, is defined by

$$T_n(r) = \left\langle \Delta v(r)^n \right\rangle. \tag{27}$$

Both $S_n(r)$ and $T_n(r)$ can be non-dimensionalized using the *n*/2 power of the variance $\left\langle u^2 \right\rangle$, and the dimensionless structures functions are denoted as $s_n(r)$ and $t_n(r)$, respectively. For isotropic turbulence, Kármán and Howarth [40] showed that the transverse and longitudinal structure functions of second order can be related by the expression

$$t_2(r) = s_2(r) + \frac{r}{2}\frac{\partial s_2(r)}{\partial r}. \tag{28}$$

A plot comparing $t_2(r)$ to the right-hand side of (28) is shown in Figure 10, where the dashed line indicates the theoretical expression (28) for isotropic turbulence. The DNS computation used 21 target points, whereas 41 target points were used for the LSVS computation. Both computations are reasonably close to the theoretical expression, although LSVS is observed to deviate from the isotropic theory for vary small or vary large values of *r*.

B. Uniformly Translated Target Points

Both DNS and LSVS computations were repeated for translating targets, with values of the target point mean translation velocity U_x ranging between 0.1 - 0.5, which is equal to 0.5 - 2.5 times the turbulence root-mean-square velocity u_0. At low values of U_x the temporal resolution of the turbulence in the LSVS model controls the model accuracy, similar to the case for a stationary target, whereas at high values of U_x the LSVS accuracy is controlled by the spatial representation of the turbulence as the target point moves through it. Examination of different statistical measures of the predicted LSVS results indicate that target point translation has little affect on several of the measures presented in the previous section, including the probability density function, the power spectrum, and the Eulerian structure function $S_n(r)$. However, the autocorrelation function $\rho(\tau)$ exhibits significant sensitivity to translation velocity.

A demonstration of the sensitivity of the autocorrelation to target point translation is shown in Figure 11a, in which the autocorrelation function $\rho(\tau)$ is plotted versus lag time τ for a series of four LSVS computations with U_x = 0, 0.1, 0.3 and 0.5. The highest translation velocity is about 2.5 times the root-mean square velocity u_0 of the turbulent flow. The value

autocorrelation function is seen to monotonically decrease as the translation velocity is increased. A similar trend is observed in Figure 11b, which plots the integral time scale T_L obtained from (22) as a function of target point translation velocity U_x. The value of T_L is monotonically decreases as U_x increases. These observations are consistent with the notion that translation of the target point relative to the turbulence increases the frequency of velocity fluctuation, thereby decreasing correlation of the velocity with its value at a previous time.

IV. Conclusions

There exists a need in simulator technology for rapid, accurate generation of synthetic turbulence on an object traveling within the turbulent flow. The method should be able to function under a prescribed turbulence mean velocity and Reynolds stress field, and it should provide a representation of the turbulence that is both temporally and structurally accurate so as to capture the change in fluctuation statistics with object translation speed relative to the turbulent flow. A simple method to achieve this aim is proposed in the current paper, based on the idea of finite-length vortex structures that are advected and rotated in the flow field via solution of stochastic differential equations of the Langevin type. The proposed method is an extension of the stochastic vortex structure (SVS) method recently developed for particulate flows, which has been demonstrated to provide correct prediction of particle collision rate, as well as a wide range of particle dispersion and agglomeration statistics, in both homogeneous turbulence and turbulent shear flows. However, the standard SVS method computes the turbulent fluctuations on a grid covering the entire computational domain and advects the vortex structures by interpolation of the velocity computed on this grid. Even with the use of acceleration methods such as the fast multipole method, the standard SVS method is far too slow for simulator

applications due to the large number of grid points on which the velocity is computed. The use of stochastic differential equations for vortex motion and rotation and of a restricted vortex region in the local stochastic vortex structure (LSVS) method developed in the current paper dramatically speeds up the synthetic turbulence computation for the flight simulator problem.

Predictions of the new LSVS method were validated for a wide range of statistical measures by comparison to results for direct numerical simulation (DNS) of homogeneous turbulence. Bearing in mind the fact that the proposed LSVS method was developed to achieve a rapid synthetic turbulence calculation that can only be expected to be statistically similar to actual turbulence, the agreement with DNS predictions was found to be quite encouraging. The LSVS predictions yield a probability density function for velocity that is reasonably close to DNS predictions. The predicted power spectrum agreed with the DNS results at low frequencies ($f < 30$) and with the expected $\sim f^{-5/3}$ Kolmogorov dependence within the inertial subrange. The autocorrelation function, as well as the associated Lagrangian structure function, were shown to be sensitive to the vortex lifetime and, to a lesser extent, to vortex translation within the flow field. Good agreement of the LSVS results with DNS predictions and with the expected exponential decay formula for the autocorrelation was obtained when the vortex lifetime was set to approximately three times the eddy turnover time scale. The Eulerian structure function is found to be sensitive to the vortex core radius. Excellent agreement between the LSVS results and the DNS predictions was obtained by setting the vortex core radius to eight times the Kolmogorov length scale.

While the results presented in this paper show promise for use of the LSVS method for flight simulator synthetic turbulence generation, additional steps are necessary to achieve this objective. It is envisioned that a typical simulator application would first involve a computation

of the Reynolds-averaged turbulence field, using a standard RANS method, leading to prediction of the Reynolds stress tensor within the flow field. The predicted turbulence from the RANS computation would be formed both by the ambient atmospheric turbulence and the wake turbulence of large-scale bodies present in the simulator (e.g., ships, building, topography), where in the latter case it would typically include large-scale wake vortices. The SVS vortices responsible for generating the synthetic turbulence fluctuations would then be initialized to match the computed (anisotropic) Reynolds stress tensor using the inverse procedure described by Dizaji et al. [28]. The same procedure would be used to generate new vortices as existing vortices die out during the flow computation. In principle, the same approach could be used for unsteady RANS calculations (e.g., in the presence of large-scale wake vortices from large bodies in the flow field), and in this case the inverse procedure described by Dizaji et al. [28] would need to be updated at each time step.

Funding Sources

This research was supported by the U.S. National Science Foundation under grant CBET-1332472.

References

[1] Polsky, S. A., Wilkinson, C., Nichols, J., Ayers, D., Mercado-Perez, J., and Davis, T. S., "Development and Application of the SAFEDI Tool for Virtual Dynamic Interface Ship Airwake Analysis," *54th AIAA Aerospace Sciences Meeting*, AIAA paper 2016-1771, 2016.

[2] Xin, H. and He, C., "A Statistical Turbulence Model for Shipboard Rotorcraft Simulations," *American Helicopter Society 63rd Annual Forum*, Virginia Beach, May 1-3, 2007.

[3] Pope, S. B., "Simple Models of Turbulent Flows," *Physics of Fluids*, Vol. 23, 2011, Paper 011301.

[4] Thomson, D. J., "Criteria for the Selection of Stochastic Models of Particle Trajectories in Turbulent Flows," *Journal of Fluid Mechanics*, Vol. 180, 1987, pp. 529-556.

[5] Minier, J. P., Chibbaro, C., and Pope, S.B., "Guidelines for the Formulation of Lagrangian Stochastic Models for Particle Simulations of Single-Phase and Dispersed Two-Phase Flows," *Physics of Fluids*, Vol. 26, 2014, Paper 113303.

[6] Sala, K. and Marshall, J. S., "Stochastic Vortex Structure Method for Modeling Particle Clustering and Collisions in Homogeneous Turbulence," *Physics of Fluids*, Vol. 25, No. 10, 2013, Paper 103301.

[7] Batten, P., Goldberg, U., and Chakravarthy, S., "Interfacing Statistical Turbulence Closures with Large-Eddy Simulation," *AIAA Journal*, Vol. 42, No. 3, 2004, pp. 485-492.

[8] Castro, H. G., and Paz, R. R., "A Time and Space Correlated Turbulence Synthesis Method for Large Eddy Simulations," *Journal of Computational Physics*, Vol. 235, 2013, pp. 742-763.

[9] Lund, T. S., Wu, X., and Squires, K. D., "Generation of Turbulent Inflow Data for Spatially-Developing Boundary Layer Simulations," *Journal of Computational Physics*, Vol. 140, 1998, pp. 233-258.

[10] Kraichnan, R. H., "Diffusion by a Random Velocity Field," *Physics of Fluids*, Vol. 13, 1970, pp. 22-31.

[11] Smirnov, A., Shi, S., and Celik, I., "Random Flow Generation Technique for Large Eddy Simulations and Particle-Dynamics Modeling," *Journal of Fluids Engineering*, Vol. 123, 2001, pp. 359-371.

[12] Huang, S. H., Li, Q. S., and Wu, J. R., "A General Inflow Turbulence Generator for Large Eddy Simulation," *Journal of Wind Engineering and Industrial Aerodynamics*, Vol. 98, 2010, pp. 600-617.

[13] Tabor, G. R., and Baba-Ahmadi, M. H., "Inlet Conditions for Large Eddy Simulation: A Review," *Computers & Fluids*, Vol. 39, 2010, pp. 553-567.

[14] Jiménez, J., Wray, A. A., Saffman, P. G., and Rogallo, R. S., "The Structure of Intense Vorticity in Isotropic Turbulence," *Journal of Fluid Mechanics*, Vol. 255, 1993, pp. 65-90.

[15] Berlin, F., Maurer, J., Tabeling, P., and Willaime, H., "Observation of Intense Filaments In Fully Developed Turbulence," *Journal de Physique II France*, Vol. 6, 1996, pp. 73-585.

[16] Townsend, A. A., "On the Fine Scale of Turbulence," *Proceedings of the Royal Society of London A*, Vol. 208, 1951, pp. 534-542.

[17] Pullin, D. I., and Saffman, P. G., "On the Lundgren-Townsend Model of Turbulent Fine Scales," *Physics of Fluids*, Vol. 5, No. 1, 1993, pp. 126-145.

[18] Malik, N. A., and Vassilicos, J. C., "Eulerian and Lagrangian Scaling Properties of Randomly Advected Vortex Tubes," *Journal of Fluid Mechanics*, Vol. 326, 1996, pp. 417-436.

[19] Min, I. A., Mezić, I., and Leonard, A., "Lévy Stable Distributions for Velocity and Vorticity Difference in Systems of Vortex Elements," *Physics of Fluids*, Vol. 8, 1996, pp. 1169-1180.

[20] Saffman, P. G., "Vortex Models of Isotropic Turbulence," *Philosophical Transactions of the Royal Society of London A*, Vol. 355, 1997, pp. 1949-1956.

[21] Wilczek, M., Jenko, F., and Friedrich, R., "Lagrangian Particle Statistics in Turbulent Flows from a Simple Vortex Model," *Physical Review E*, Vol. 77, 2008, Paper 056301.

[22] Kivotides, D., and Leonard, A., "Quantized Turbulence Physics," *Physical Review Letters*, Vol. 90, No. 23, 2003, Paper 234503.

[23] Bernard, P. S., "Grid-free Simulation of the Spatially Growing Turbulent Mixing Layer," *AIAA Journal*, Vol. 46, No. 7, 2008, pp. 1725-1737.

[24] Bernard, P. S., "Vortex Filament Simulation of the Turbulent Coflowing Jet," *Physics of Fluids*, Vol. 21, 2009, Paper 025107.

[25] Bernard, P. S., Collins, P., and Potts, M., "Vortex Filament Simulation of the Turbulent Boundary Layer," *AIAA Journal*, Vol. 48, No. 8, 2010, pp. 1757-1771.

[26] Ayyalasomayajula, S., Warhaft, Z., and Collins, L. R., "Modeling Inertial Particle Acceleration Statistics in Isotropic Turbulence," *Physics of Fluids*, Vol. 20, 2008, Paper 095104.

[27] Dizaji, F. F., and Marshall, J. S., "An Accelerated Stochastic Vortex Structure Method for Particle Collision and Agglomeration in Homogeneous Turbulence," *Physics of Fluids*, Vol. 28, 2016, Paper 113301.

[28] Dizaji, F. F., Marshall, J. S., and Grant, J. R., "A Stochastic Vortex Structure Method for Interacting Particles in Turbulent Shear Flows," *Physics of Fluids*, Vol. 30, 2018, Paper 013301.

[29] La Porta, A., Voth, G. A., Crawford, A. M., Alexander, J., and Bodenschatz, E., "Fluid Particle Acceleration in Fully Developed Turbulence," *Nature*, Vol. 409, 2001, pp. 1017-1019.

[30] Vassilicos, J. C., "Dissipation in Turbulent Flows," *Annual Review of Fluid Mechanics*, Vol. 47, 2015, pp. 95-114.

[31] Kambe, T., and Hatakeyama, N., "Statistical Laws and Vortex Structures in Fully Developed Turbulence," *Fluid Dynamics Research*, Vol. 27, 2000, pp. 247-267.

[32] Hughes, P. C., *Spacecraft Attitude Dynamics*, John Wiley & Sons, Inc., New York, 1986.

[33] Marshall, J. S. and Grant, J. R., "Penetration of a Blade into a Vortex Core: Vorticity Response and Unsteady Blade Forces," *Journal of Fluid Mechanics*, Vol. 306, 1996, pp. 83-109.

[34] Abramowitz, M., and Stegun, I. A., *Handbook of Mathematical Functions*, Dover Publ., New York, 1965.

[35] Vincent, A., and Meneguzzi, M., "The Spatial Structure and Statistical Properties of Homogeneous Turbulence," *Journal of Fluid Mechanics*, Vol. 225, 1991, pp. 1-20.

[36] Lundgren, T. S., "Linearly Forced Isotropic Turbulence," Annual Research Briefs, CTR, Stanford, 2003, pp. 461-473.

[37] Rosales, C., and Meneveau, C., "Linear Forcing in Numerical Simulations of Isotropic Turbulence: Physical Space Implementations and Convergence Properties," *Physics of Fluids*, Vol. 17, No. 9, 2005, Paper 095106.

[38] Cruz, F. A., Knepley, M. G., and Barba, L. A., "Fast Multipole Method for Particle Interactions: An Open Source Parallel Library Component," In *Parallel Computational Fluid Dynamics 2008*, D. Tromeur-Dervout (eds.), Lecture Notes in Computational Science and Engineering, Vol. 74, Springer-Verlag Berlin Heidelberg, 2010.

[39] Pope, S. B., *Turbulence Flows*, Cambridge University Press, Cambridge, U.K., 2000, p. 485.

[40] de Kármán, T., and Howarth, L., "On the Statistical Theory of Isotropic Turbulence," *Proceedings of the Royal Society of London A*, Vol. 164, No. 917, 1938, pp. 192-215.

Figure Captions

Figure 1. Schematic diagram showing the computational domain, the set of target points that move through the flow field, and the vortex domain in which stochastic vortex structures are placed to generate fluctuating turbulence at the target points.

Figure 2. Schematic diagram showing the interpolation procedure used for direct computation of the velocity induced by a vortex structure on a target point. Here L is the length of the vortex structure and P identifies the inclined data plane from which the velocity **u** induced by the vortex is interpolated.

Figure 3. CPU time (in μs) per time step per target point for the LSVS computation plotted as a function of the number of vortex structures.

Figure 4. Time series showing the fluctuating fluid velocity at the central target point for (a) DNS and (B) LSVS methods.

Figure 5. Probability density function for the x-component of velocity at the central target point, obtained for LSVS (open squares), DNS (filled deltas), and a best-fit Gaussian curve.

Figure 6. Power spectrum as a function of frequency for the LSVS (red) and DNS (blue) data. The inertial-range $\sim f^{-5/3}$ dependence is indicated using a dashed line.

Figure 7. Plots showing (a) the autocorrelation $\rho(\tau)$ and (b) the Lagrangian structure function $D(\tau)$ as functions of the lag time τ for LSVS (open squares), DNS (filled deltas) and for the exponential empirical estimates (dashed line) given by Eqs. (23) and (25).

Figure 8. Plots examining sensitivity of the autocorrelation function predicted by the LSVS method to (a) vortex lifetime [with proportionality coefficient values $\alpha_3 = 1$ (A, red line), 3 (B, blue line), and 5 (C, green line)], (b) vortex motions [comparing case B to computations with no vortex motion (D, solid black line) and to computations with translation but no vortex rotation (E, dashed line)], and (c) vortex bouncing [comparing case B to a computation with no vortex bouncing (F, orange line)].

Figure 9. Eulerian longitudinal structure function $S_n(r)$ as a function of offset distance r for LSVS (lines) and DNS (symbols), with order $n = 2$ (red line, squares), 4 (blue line, deltas), 6 (green line, gradients), 8 (orange line, diamonds), and 10 (black line, circles). Plots show sensitivity to the vortex core proportionality parameter, with (a) $\alpha_2 = 4$ and (b) $\alpha_2 = 8$.

Figure 10. Plot comparing the second-order Eulerian transverse structure function $t_2(r)$ to the right-hand side of Eq. (28) for the DNS computation (deltas) and for an LSVS computation (circles). The theoretical expression for isotropic turbulence is indicated by a dashed line.

Figure 11. Plot showing (a) the autocorrelation function and (b) the corresponding integral time scale on translated target points from LSVS computations. The target point translation velocity is given by $U_x = 0$ (A, red line), 0.1 (B, green line), 0.3 (C, blue line) and 0.5 (D, black line).

Table 1. Scaling variables charaterizing the fluid turbulence in the DNS computation.

Turbulent kinetic energy, q	0.084	Taylor microscale, λ	0.23
Root-mean square velocity fluctuation, u_0	0.24	Microscale Reynolds number, Re_λ	56
Mean dissipation rate, ε	0.016	Integral length, ℓ_0	0.86
Kinematic viscosity, ν	0.001	Eddy turnover time, T_0	3.6
Kolmogorov length scale, η	0.016	Integral time, T_ℓ	2.8

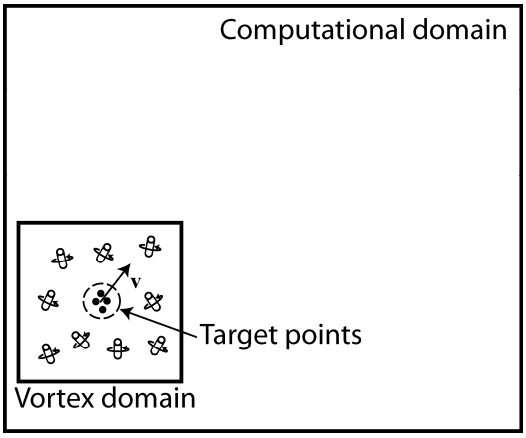

Figure 1. Schematic diagram showing the computational domain, the set of target points that move through the flow field, and the vortex domain in which stochastic vortex structures are placed to generate fluctuating turbulence at the target points.

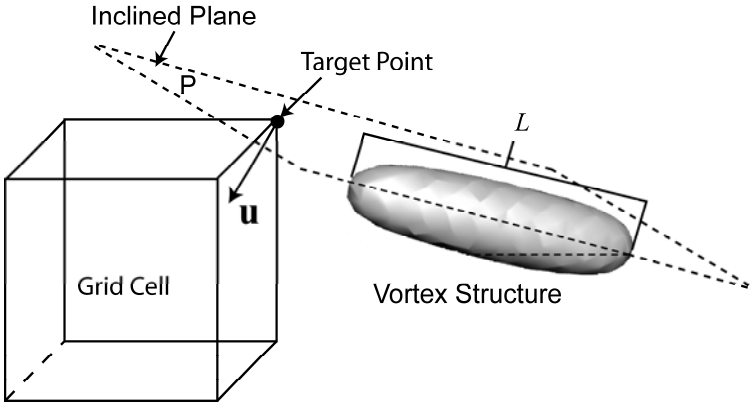

Figure 2. Schematic diagram showing the interpolation procedure used for direct computation of the velocity induced by a vortex structure on a target point. Here L is the length of the vortex structure and P identifies the inclined data plane from which the velocity **u** induced by the vortex is interpolated.

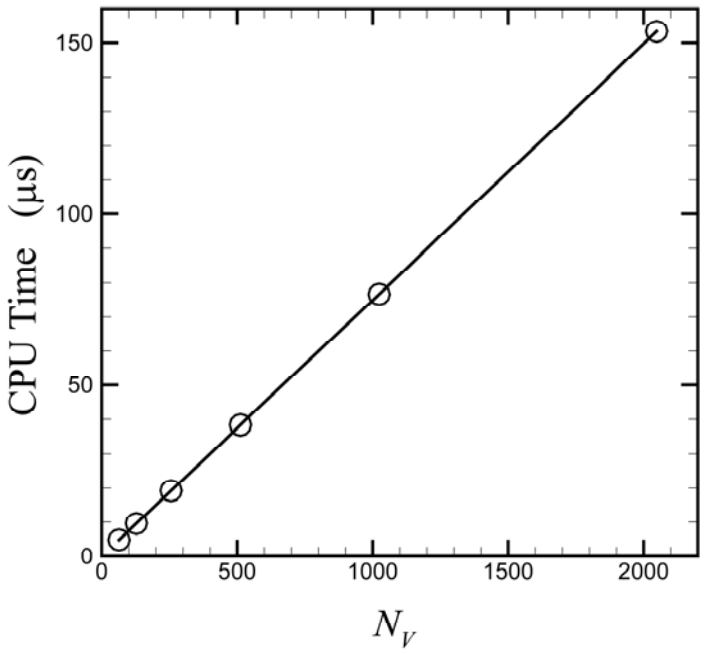

Figure 3. CPU time (in μs) per time step per target point for the LSVS computation plotted as a function of the number of vortex structures.

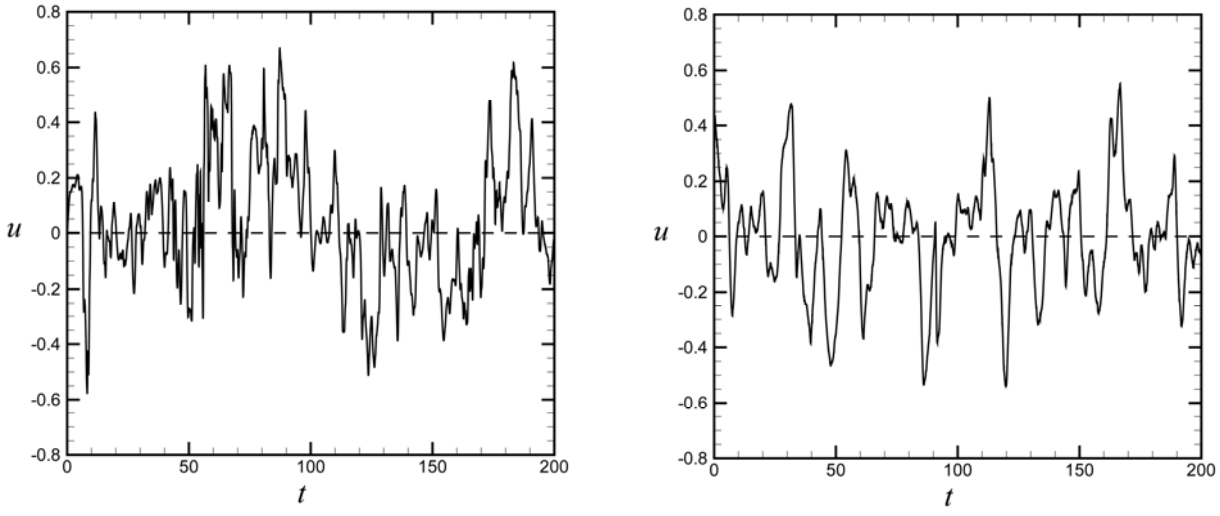

Figure 4. Time series showing the fluctuating fluid velocity at the central target point for (a) DNS and (B) LSVS methods.

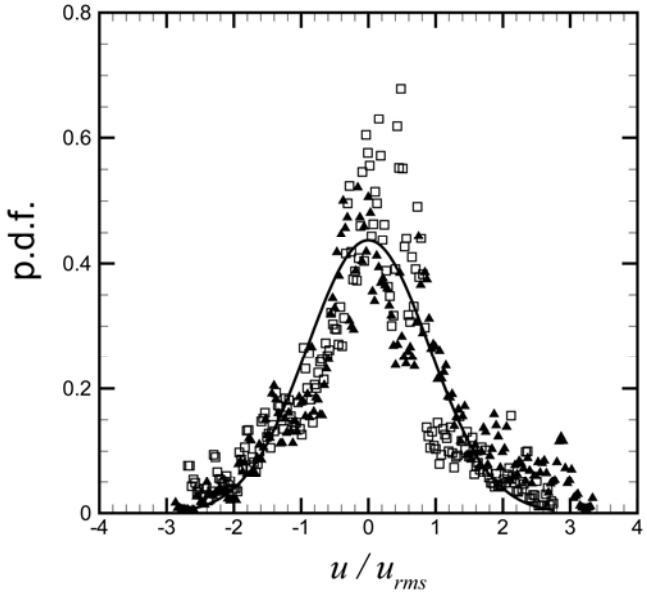

Figure 5. Probability density function for the *x*-component of velocity at the central target point, obtained for LSVS (open squares), DNS (filled deltas), and a best-fit Gaussian curve.

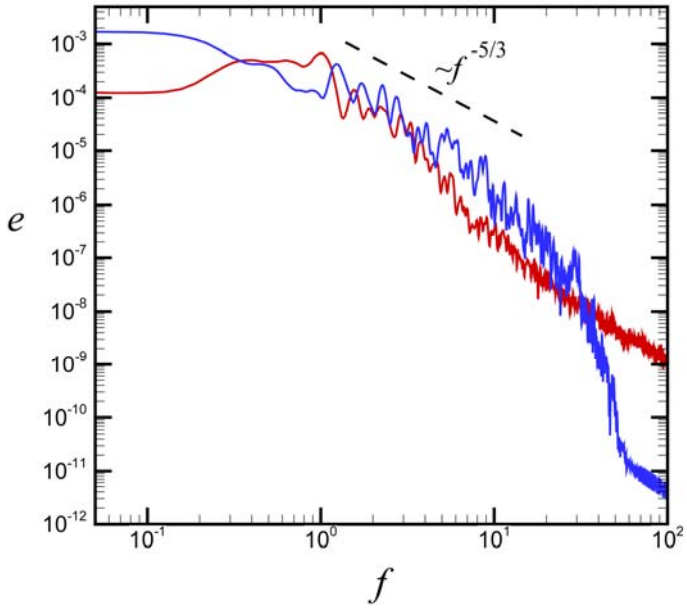

Figure 6. Power spectrum as a function of frequency for the LSVS (red) and DNS (blue) data. The inertial-range $\sim f^{-5/3}$ dependence is indicated using a dashed line.

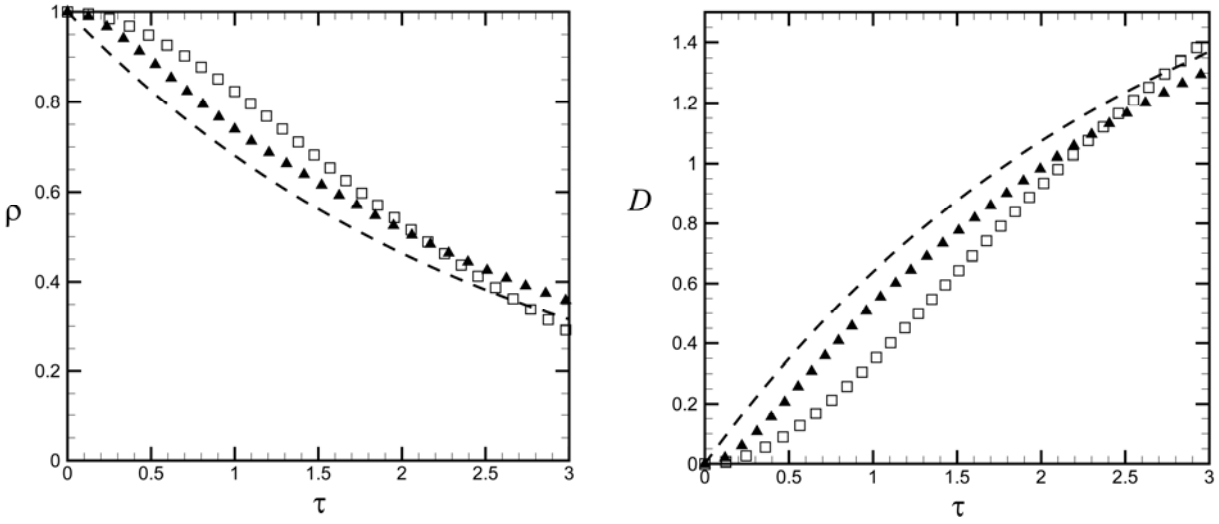

(a) (b)

Figure 7. Plots showing (a) the autocorrelation $\rho(\tau)$ and (b) the Lagrangian structure function $D(\tau)$ as functions of the lag time τ for LSVS (open squares), DNS (filled deltas) and for the exponential empirical estimates (dashed line) given by Eqs. (23) and (25).

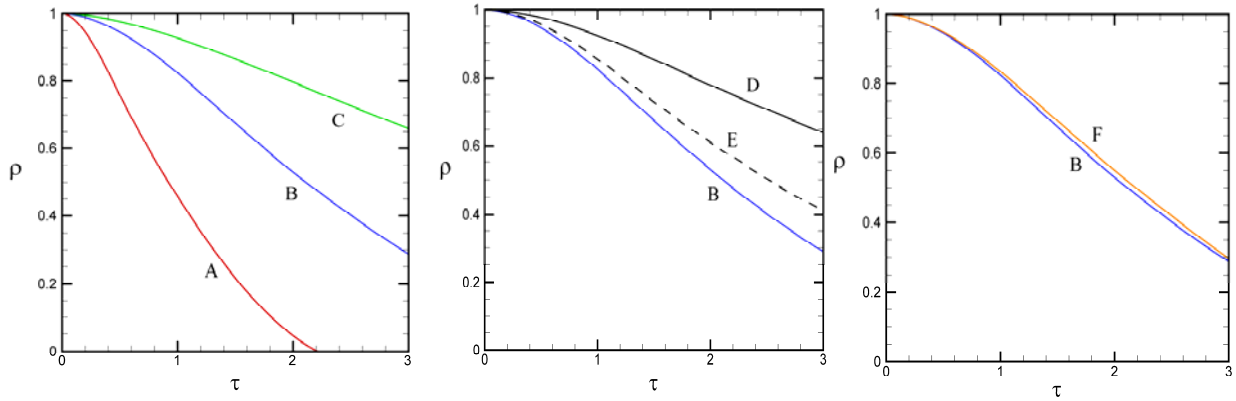

(a) (b) (c)

Figure 8. Plots examining sensitivity of the autocorrelation function predicted by the LSVS method to (a) vortex lifetime [with proportionality coefficient values $\alpha_3 = 1$ (A, red line), 3 (B, blue line), and 5 (C, green line)], (b) vortex motions [comparing case B to computations with no vortex motion (D, solid black line) and to computations with translation but no vortex rotation (E, dashed line)], and (c) vortex bouncing [comparing case B to a computation with no vortex bouncing (F, orange line)].

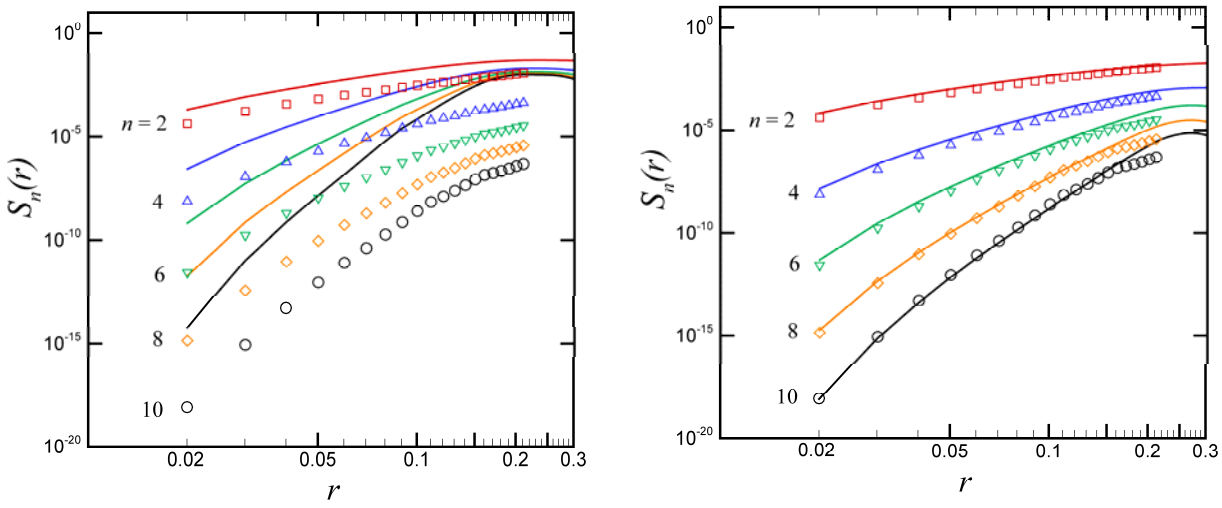

Figure 9. Eulerian longitudinal structure function $S_n(r)$ as a function of offset distance r for LSVS (lines) and DNS (symbols), with order $n=2$ (red line, squares), 4 (blue line, deltas), 6 (green line, gradients), 8 (orange line, diamonds), and 10 (black line, circles). Plots show sensitivity to the vortex core proportionality parameter, with (a) $\alpha_2 = 4$ and (b) $\alpha_2 = 8$.

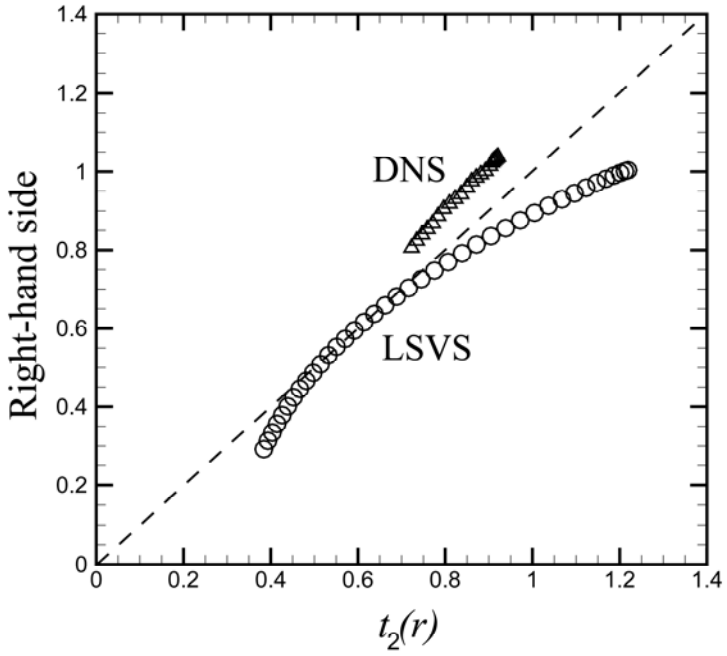

Figure 10. Plot comparing the second-order Eulerian transverse structure function $t_2(r)$ to the right-hand side of Eq. (28) for the DNS computation (deltas) and for an LSVS computation (circles). The theoretical expression for isotropic turbulence is indicated by a dashed line.

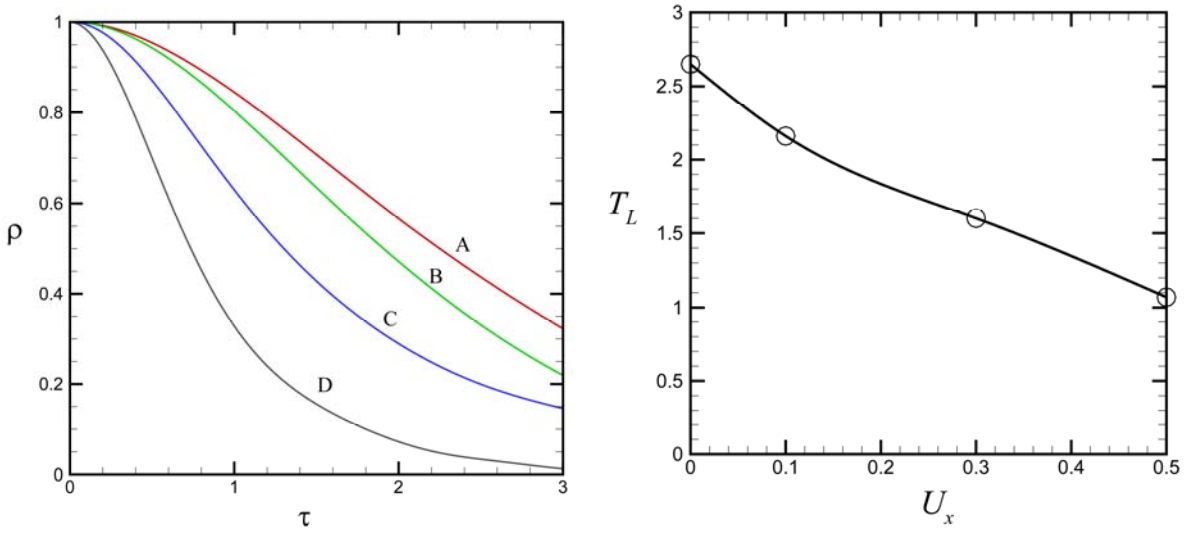

(a) (b)

Figure 11. Plot showing (a) the autocorrelation function and (b) the corresponding integral time scale on translated target points from LSVS computations. The target point translation velocity is given by $U_x = 0$ (A, red line), 0.1 (B, green line), 0.3 (C, blue line) and 0.5 (D, black line).